Conformational Properties of DNA Hairpins with TTT and TTTT Loops

Susan M. Baxter,‡ Miriam B. Greizerstein, Diana M. Kushlan, and Gary W. Ashley*

Department of Chemistry, Northwestern University, Evanston, Illinois 60208

Received February 10, 1993; Revised Manuscript Received June 2, 1993

ABSTRACT: The DNA hairpins d[CGATCG-T_n-CGATCG] (n = 3, 4) have been studied by NMR in order to gain information on hairpin conformation and flexibility. Resonance assignments were made using a combination of DQF-COSY, DQF-COSY{^{31}P}, NOESY, and ^{1}H–^{31}P-COSY. These data also provide approximate coupling constant information which points out exceptionally flexible regions of the phosphate backbone. The data for both hairpins reveal substantial flexibility within the loop segments. For n = 4, NOESY data alone are insufficient to distinguish between two loop-folding motifs, although coupling constant data favor a conformation in which T_b is folded toward the minor groove and is highly exposed to solvent. This is in agreement with chemical shift data and susceptibility to modification by $KMnO_4$. The phosphate backbone between T_c and T_d is exceptionally flexible, undergoing a facile exchange between (β^t,γ^+) and (β^+,γ^t) conformers. A similar flexible phosphate is observed between T_c and C7 when n = 3. Differences in stem conformation and dynamics in both hairpins are restricted to the two base pairs adjacent to the stem–loop junction. The C7pG8 stem phosphate appears to flip easily between (ζ^-,α^-) and (ζ^-,α^t) conformers when n = 4 but not when n = 3. Hairpin loop size thus affects the conformational flexibility of the adjacent stem segment.

Hairpin loops are among the most prevalent noncanonical nucleic acid conformations, occurring frequently in RNA secondary structures and in DNA cruciforms. As such they have received a great deal of attention in terms of their conformational and biochemical properties. A clear understanding of the relationships between hairpin loop size, structure, and the effects of these parameters on the conformations of the connected double-helical stem segments remains elusive, however.

The existence of such structure/activity relationships is made clear by investigations relating the influence of hairpin loop size on the ability of restriction enzymes to cleave within the stem (Germann et al., 1990; Amaratunga et al., 1992), the activity of DNA ligase on the stem (Erie et al., 1989), and the thermodynamic and spectral properties of the duplex (Amaratunga et al., 1992; Paner et al., 1992). It has been postulated that the hairpin loops induce structural distortions in the helical stem which may extend for several base pairs, yet structural evidence for such distortions is lacking. We report here an investigation of two DNA hairpins having equivalent stem sequences and loop compositions but having different loop sizes, d[CGATCG-T_n-CGATCG], where n = 3 or 4 (T3L and T4L,[1] respectively; Figure 1). Oligomers with self-complementary end sequences containing unpaired central stretches of thymidines form stable hairpins (Senior et al., 1988), and the TTT and TTTT loops are representative of loop sizes which either do or do not, respectively, affect restriction cleavage within the adjacent stem (Germann et al., 1990). We report data indicating significant differences in the conformational flexibility of the stem segments of these two hairpins, suggesting structural interactions between the step and loop. The observed effects of loop size on the biological properties of DNA hairpins may reflect alterations in adjacent stem dynamics as well as structural distortions.

MATERIALS AND METHODS

DNA Synthesis. DNA oligomers were prepared by automated cyanoethyl phosphoramidite synthesis at the NU Biotechnology Facility. Crude DNA was purified by anion-exchange chromatography on Sepharose QFF using a linear gradient from 0.2 to 0.8 M NaCl in 10 mM NaOH. After neutralization with dilute HCl to pH 7, the DNA was concentrated and desalted by absorption onto C_{18} cartridges (Alltech Maxi-Clean).

NMR Spectroscopy. ^{1}H chemical shifts are referenced to internal TSP. ^{31}P chemical shifts are referenced to external 85% H_3PO_4 set to –0.73 ppm (Tebby, 1987). NMR samples in D_2O were prepared by repeated evaporation from 99.8 atom % *d* D_2O followed by dissolution in 99.998 atom % *d* D_2O. NMR samples consisted of 3.9 mM strands for T3L and 2.8 mM strands for T4L, both in the Na^+ form unbuffered at pH 7 with no added NaCl. Spectra were obtained on a Bruker AMX-600 spectrometer operating at 600 MHz for ^{1}H and 220 MHz for ^{31}P using the method of States et al. (1982). Samples were thermostated at 298.1 K unless otherwise noted. NOESY spectra were collected with 4K × 1K complex points over a width of 6024 Hz using 32 transients per FID and a relaxation delay of 2.5 s. Mix times of 50, 100, and 200 ms were used. The data set was zero-filled in t_1 to 2K × 1K real points and weighted with an exponential multiplier (1-Hz line broadening) prior to transformation. The DQF-COSY and DQF-COSY{^{31}P} data sets were collected with 8K × 2K complex points and a relaxation delay of 1.5 s, zero-filled in t_1 to 4K × 2K real points, and weighted with a Gaussian function in t_2 and a skewed sine bell in t_1 prior to transformation. The DQF-COSY{^{31}P} spectrum was acquired using

‡ Present address: Institute of Molecular Biology, University of Oregon, Eugene, OR 97403.

[1] Abbreviations: T3L, d[CGATCG-TTT-CGATCG]; T4L, d[CGATCG-TTTT-CGATCG]; DQF-COSY, 2D double-quantum-filtered correlation spectroscopy; DQF-COSY{^{31}P}, 2D double-quantum-filtered correlation spectroscopy with broad-band ^{31}P decoupling; NOESY, 2D nuclear Overhauser exchange spectroscopy; HP-COSY, ^{1}H–^{31}P inverse-detected heteronuclear correlation spectroscopy; H5′, the *pro-S* proton of C5′; H5″, the *pro-R* proton of C5′; ISPA, independent spin pair analysis; RMS_{vol}(exp), the root mean square of the percent difference between the calculated and experimental NOESY volumes based on the experimental volumes; RMS_{vol}(the), the root mean square of the percent difference between the calculated and experimental NOESY volumes based on the theoretical volumes.

0006-2960/93/0432-8702$04.00/0

continuous GARP decoupling for ^{31}P. The HP-COSY experiment (Sklenar et al., 1986) was collected with 4K × 256 complex points and zero-filled to 2K × 512 real points prior to transformation. Spectra were processed using Felix (Hare Research, Woodinville, WA).

Model Building. Initial hairpin models were constructed using Quanta (Molecular Simulations, Inc.) from standard B-DNA parameters using the Amber force field with a distance-dependent dielectric constant (Kollman et al., 1981). Initial conformers were generated by application of ISPA-derived distances from 50-, 100-, and 200-ms NOESY experiments as flat-well potential constraints (Gorenstein et al., 1990) in constrained quenched molecular dynamics (500–100 K over 5 ps) followed by energy minimization. The resulting structures were used to back-calculate the expected NOESY spectrum for t_{mix} = 100 ms and τ_c = 2.0 ns using the program MORASS (Nikonowicz et al., 1990). A hybrid volume matrix was prepared by substitution with experimental volumes scaled by a factor empirically determined to best reproduce resolved diagonal, H2′–H2″, and dC H5–H6 cross-peak volumes. This hybrid volume matrix was used to calculate a rate matrix and corresponding interproton distances, which were then applied to the model through quenched molecular dynamics and energy minimization. This process was repeated until no further improvement in the agreement between the experimental and theoretical NOESY volumes was obtained. Final models showed the following fits between calculated and experimental NOESY volumes, with root mean square volume errors in percent against the experimental data (RMS_{vol}(exp)) and against the theoretical volumes (RMS_{vol}(the)) and *R*-factors: T3L, RMS_{vol}(exp) = 50%, RMS_{vol}(the) = 46%, and R = 14%; T4L-1, RMS_{vol}(exp) = 45%, RMS_{vol}(the) = 38%, and R = 20%.

RESULTS

Confirmation of Hairpin Formation. Optical melting, chemical modification, and NMR experiments suggested that both T3L and T4L exist essentially exclusively as hairpins under the conditions of these experiments. Optical melting experiments revealed single hyperchromic transitions, with T_m = 70 °C for both molecules at pH 7 in 0.1 M NaCl. The T_m for these transitions was independent of DNA concentration, indicative of a unimolecular melting process. No evidence for a second transition due to bulged dimer formation could be observed. The loop thymidines were hypersensitive to oxidation by $KMnO_4$ (Williamson & Celander, 1990) as expected for nonpaired loop residues. Finally, the correlation times determined from NOESY buildup curves for cytosine H5–H6 cross-peaks relative to that observed for a known 10-mer duplex indicated structures of length equivalent to approximately seven base pairs, consistent with hairpin structures. No minor cross-peaks which might indicate the presence of a small amount of bulged duplex were observed in any of the 2D-NMR spectra.

NMR Resonance Assignments. To simplify comparison of T3L and T4L, a labeling scheme is adopted in which the stem residues are numbered C1 through G6 and C7 through G12, while the loop T residues are labeled T_a, T_b, and T_c from 5′ to 3′ in T3L and T_a, T_b, T_c, and T_d from 5′ to 3′ in T4L (Figure 1). Thus, C7 refers to the initial dC residues on the 3′ side of the stem–loop junction in both molecules.

Resonance assignments were made using a combination of NOESY, DQF-COSY, and DQF-COSY{^{31}P} spectra. Sequential assignments of H8, H6, H5, H1′, H2′, H2″, and H3′ were made using standard methodology (Hare et al., 1983; Chazin et al., 1986). H4′ signals were assigned from the H3′/H4′ cross-peaks in the DQF-COSY spectrum, with assistance from the H1′–H4′ cross-peaks in the NOESY spectrum. Where this was ambiguous due to overlap of H3′ chemical shifts, the HP-COSY spectra (Figure 2) were used to relate the H3′ of the 5′ neighbor with H4′. H5′/H5″ were assigned similarly. With the increased resolution available in the DQF-COSY{^{31}P} spectrum, most of these assignments could be made unambiguously (Table I).

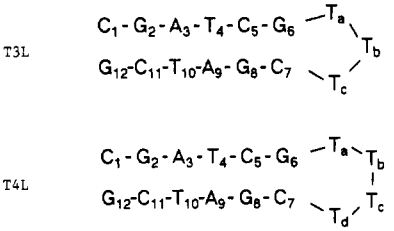

FIGURE 1: Nomenclature for T3L (top) and T4L (bottom) DNA hairpins.

As nearly all γ torsions can be confined to γ^+ (γ = 60°) on the basis of the observation of small, near-equivalent H4′–H5′ and H4′–H5″ antiphase separations in the DQF-COSY-{^{31}P} spectra (Figure 3), comparison of relative NOESY intensities for H5′/H5″ to H3′, H2′, and H6 resonances allows stereospecific assignment of H5′ (*pro-S*) and H5″ (*pro-R*) where signal resolution permits. In T3L, H5′/H5″ could not be unambiguously distinguished for T_b due to overlap of one signal with that for H4′, although the assignment indicated is plausible on the basis of the intensity of the resolved peak relative to those of other residues.

Assignment of the loop thymidines in T3L was ambiguous due to the lack of sequential H8/H6:H2′/H2″ NOEs in this region, although weak H8/H6:H1′ NOEs were observed. The HP-COSY spectrum allowed clear assignments by means of internucleotide connectivities between the H3′ of one nucleotide and the H5′/H5″/H4′ of the 3′-neighbor nucleotide through the phosphates, even though the H3′ resonances of T_a and T_c overlap. The thymidine H5′/H5″ signals at δ 3.83 and 3.77 are clearly correlated with a unique loop thymidine H3′ signal at δ 4.68 through the phosphorus at δ_P −1.28. The DQF-COSY{^{31}P} spectrum shows an intranucleotide connectivity between the H3′ at 4.68 and the H5′/H5″ signals at δ 3.92 and 3.98. These signals thus define a 5′-TT-3′ dinucleotide unit. The H5′/H5″ signals at δ 3.92 and 3.98 are in turn correlated through the phosphate at δ_P −1.65 with one of the δ 4.73 H3′ signals from another loop thymidine; there are no other H3′ signals at this frequency other than for C1, so this must be from T_a. Thus, the sequential assignments are set as given in Table I. This assignment matches that predicted on the basis of the H8/H6:H1′ NOESY connectivities, indicating that the NOESY cross-peaks in this region are those expected from sequential nucleotide interactions.

The resonances for the stem residue protons and phosphorus in T3L and T4L are nearly isochronous until the stem–loop junction is approached. Substantial deviations (>0.02 ppm) in the ^1H frequencies for the two hairpins are noted only for the C5·G8 and G6·C7 base pairs adjacent to the junctions, while the ^{31}P frequencies begin to deviate at the C5·G8/G6·C7 step. There is no apparent chemical shift correlation between any of the T3L and T4L loop thymidine resonances.

NOESY spectra in 80:20 H_2O–D_2O were obtained in order to probe base pairing. Exchangeable protons were assigned through NOESY connectivities to H5 resonances of dC or the methyl resonances of T. Base-paired imino protons were observed for the five base pairs G2·C11 through G6·C7 in

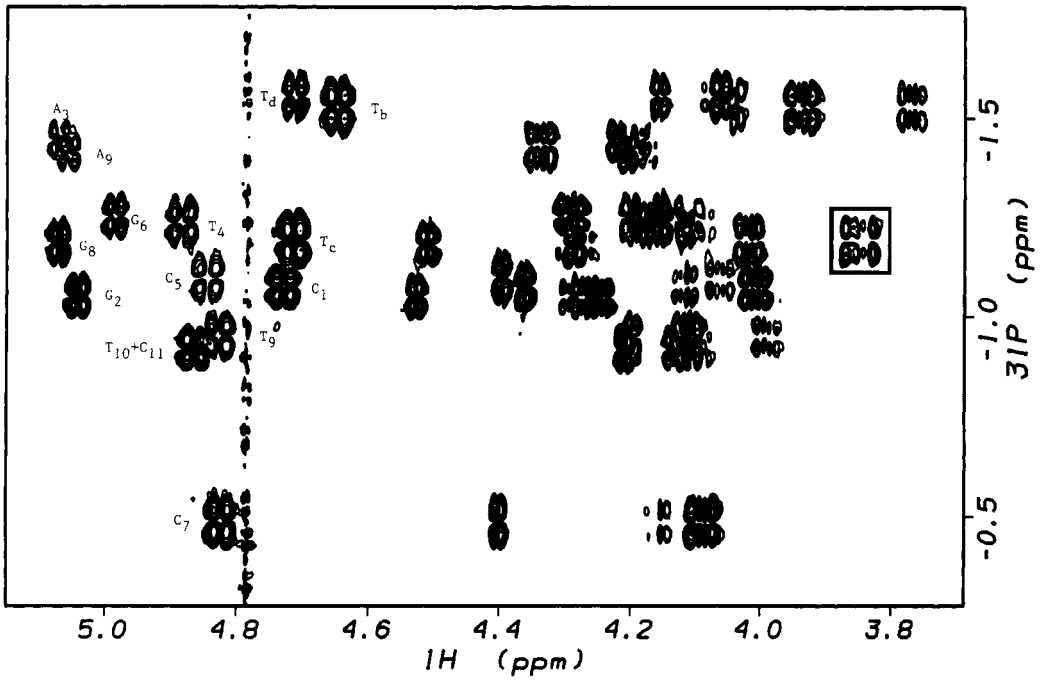

FIGURE 2: ^{1}H–^{31}P correlation spectrum for T4L. Correlations are marked from ^{31}P to H3′. The unusual cross-peak fine structure for the T_d(H5″) correlation is boxed.

Table I: Resonance Assignments for T3L and T4L[a]

residue	H6/H8	H2/H5	H1′	H2′	H2″	H3′	H4′	H5′	H5″	P
C1-3L	7.66	5.94	5.78	1.94	2.42	4.74	4.08	3.74/3.76		−1.10
C1-4L	7.65	5.96	5.77	1.94	2.42	4.73	4.08	3.73/3.76		−1.10
G2-3L	8.02		5.62	2.77	2.87	5.04	4.36	4.01/4.12		−1.08
G2-4L	8.01		5.61	2.77	2.86	5.04	4.36	4.01/4.11		−1.07
A3-3L	8.31	7.96	6.36	2.72	3.02	5.06	4.52	4.25/4.29		−1.45
A3-4L	8.31	7.94	6.35	2.72	3.01	5.06	4.53	4.24/4.28		−1.46
T4-3L	7.21	1.43	5.96	2.06	2.48	4.87	4.23	4.19/4.34		−1.20
T4-4L	7.20	1.42	5.96	2.07	2.51	4.89	4.23	4.18/4.34		−1.25
C5-3L	7.39	5.64	5.80	1.82	2.32	4.83	4.12	4.11/4.18		−1.20
C5-4L	7.40	5.66	5.76	1.85	2.33	4.84	4.12			−1.11
G6-3L	7.86		5.96	2.59	2.49	4.99	4.37	4.10/4.17		−1.02
G6-4L	7.89		6.04	2.61	2.67	4.98	4.39	4.11/4.29		−1.27
T_a-3L	7.73	1.90	6.20	2.16	2.48	4.73	4.33	4.23	4.08	−1.65
T_a-4L	7.38	1.74	6.00	2.11	2.42	4.83	4.21	4.23/4.29		−0.97
T_b-3L	7.45	1.68	5.83	2.00	2.26	4.67	3.99	3.92	3.98	−1.28
T_b-4L	7.60	1.83	6.12	2.12	2.39	4.65	4.20	3.99/4.11		−1.55
T_c-3L	7.53	1.70	6.08	2.16	2.39	4.73	4.19	3.77	3.84	−1.32
T_c-4L	7.51	1.64	5.94	2.04	2.29	4.72	4.03	3.78/3.94		−1.21
T_d-4L	7.51	1.85	6.15	2.31	2.55	4.72	4.24	4.02	3.86	−1.57
C7-3L	7.60	5.92	5.54	2.22	2.48	4.71	4.17	4.08	3.92	−0.91
C7-4L	7.61	5.86	5.34	2.20	2.41	4.82	4.16	4.06/4.13		−0.51
G8-3L	7.99		5.76	2.78	2.89	5.05	4.41	4.10/4.16		−1.16
G8-4L	7.98		5.76	2.76	2.87	5.06	4.40	4.09/4.14		−1.20
A9-3L	8.27	7.94	6.35	2.67	3.01	5.05	4.48	4.28/4.29		−1.43
A9-4L	8.27	7.90	6.34	2.68	2.99	5.05	4.51	4.29/4.29		−1.43
T10-3L	7.24	1.41	5.99	2.04	2.47	4.88	4.21	4.19/4.34		−1.26
T10-4L	7.22	1.41	5.98	2.03	2.46	4.89	4.21	4.19/4.34		−1.25
C11-3L	7.52	5.70	5.79	2.04	2.41	4.86	4.15	4.10/4.15		−0.94
C11-4L	7.51	5.72	5.78	2.01	2.41	4.87	4.15			−0.95
G12-3L	7.99		6.21	2.64	2.39	4.71	4.20	4.32		
G12-4L	7.99		6.20	2.64	2.39	4.71	4.20	4.32		

[a] When stereospecific assignments of H5′ and H5″ are made, they are indicated separately.

both T3L and T4L. The only substantial differences in chemical shift are noted at G6·C7, where the imino proton shifts differ by 0.34 ppm at 10 °C.

Variable Temperature Studies. Most stem resonances show only modest changes with temperature until melting begins (T_m = 62 °C by NMR for both hairpins), indicative of conformational stability within the stem. This transition occurs at a slightly lower T_m than in the optical melting studies described above, most likely due to the lower [Na^+] in the NMR samples, but most certainly reflects melting of the double-helical stem. The chemical shifts of the loop thymidine protons show more variation with temperature, as indicated by the behavior of the methyl resonances (Figure 4). In T3L, T_c is the only residue to show substantial changes in chemical shift with temperature below melting. The behavior of the loop residues in T4L is more complex. T_c shows a substantial change upon melting, whereas the chemical shift of T_b is relatively insensitive to changes in temperature.

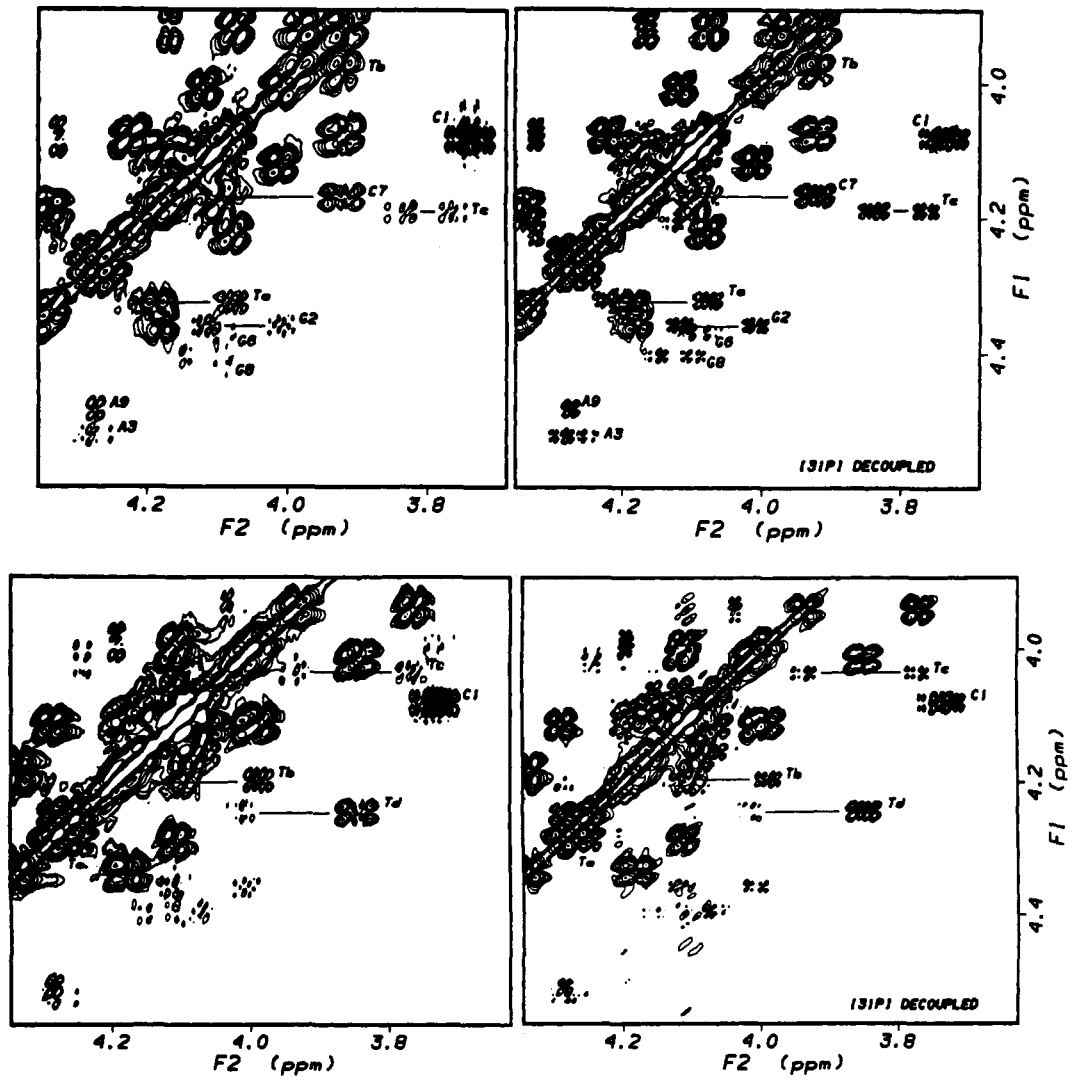

FIGURE 3: DQF-COSY (left) and DQF-COSY{^{31}P} (right) spectra for the H4′–H5′/H5″ region: (a, top) T3L; (b, bottom) T4L. Note the unusually intense cross-peaks for H4′–H5″ for C7 in T3L and for T_d in T4L. ^{31}P decoupling reveals that this is due to an unusually large H4′–H5″ coupling in both cases. The unusual cross-peak pattern for C1 in both spectra is due to overlap.

The chemical shift of H1′ in the stem residue C7 in both T3L and T4L is temperature sensitive, unlike other H1′ resonances, although the effect is much greater in T4L (5 Hz/°C) than in T3L (2 Hz/°C) (Figure 5a). A similar effect is noted for the phosphate connecting C7pG8 in T4L, which has an unusual downfield chemical shift at 25 °C. This resonance moves upfield with increasing temperature (Figure 5b). The behavior of other phosphates is less clear due to the poor resolution of the ^{31}P spectrum.

Sugar Conformations. The coupling patterns in the DQF-COSY{^{31}P} spectra indicate predominant B-form sugar parameters for all residues in both T3L and T4L. Strong H2′–H3′ cross-peaks are seen while H2″–H3′ cross-peaks are extremely weak or absent. This is true even for residues in which the relative chemical shifts for H2′ and H2″ are reversed (G12 in both T3L and T4L and G6 in T3L), indicating that this unusual chemical shift behavior is not due to a local change in sugar puckers. Measurement of the sum of couplings to H1′ for resolved resonances in the one-dimensional spectra gave values of 14.0–15.5 Hz, with $J_{1'2'}$ and $J_{1'2''}$ values indicating 85–100% S confomer for stem residues and 75% S conformer for loop thymidines (Rinkel & Altona, 1987). The relative intensities of the H3′–H4′ cross-peaks agree with this analysis (Kim et al., 1992). There are no clear differences in stem residue sugar pucker between T3L and T4L. There are no apparent changes in either $J_{1'2'}$ or $J_{1'2''}$ for C7 with temperature despite the corresponding large changes in chemical shift.

Backbone Conformations. Unusual backbone torsions are noted in both T3L and T4L. In T3L, a high proportion of the γ^t conformer (γ = 180°) is indicated for C7 on the basis of several observations: (1) there is an unusually intense H4′–H5′ cross-peak in the DQF-COSY spectrum (Figure 3a); (2) the corresponding patterns for H4′–H5′/5″ in the DQF-COSY{^{31}P} spectrum give antiphase separations of 7 and 3.5 Hz for the two H4′–H5′/5″ (Figure 3b); (3) the ^{31}P-decoupled spectrum shows $\sum J_{4'}$ = 12 Hz measured at the H3′–H4′ cross-peak, which contrasts with the more typical value of 5–6 Hz seen for all other cross-peaks; and (4) the NOESY spectrum reveals an unusually large NOE between this H5′/5″ and H6. The alternative γ^- conformer is unlikely due to the strong NOEs between H3′ and both H5′ and H5″ for this residue. The large coupling to H4′ can thus be assigned to the *pro-R* proton H5″. Calculations indicate that the pure γ^t and γ^+ conformers should show J = 10.5 and 2.6 Hz between H4′ and H5″, respectively (Haasnoot et al., 1979). The observed antiphase separation thus suggests a roughly 60:40 mix of γ^t and γ^+ conformers at C7 in T3L.

H5″ of C7 is also associated with an abnormally large J_{HP} seen as an antiphase separation of 15 Hz in the HP-COSY

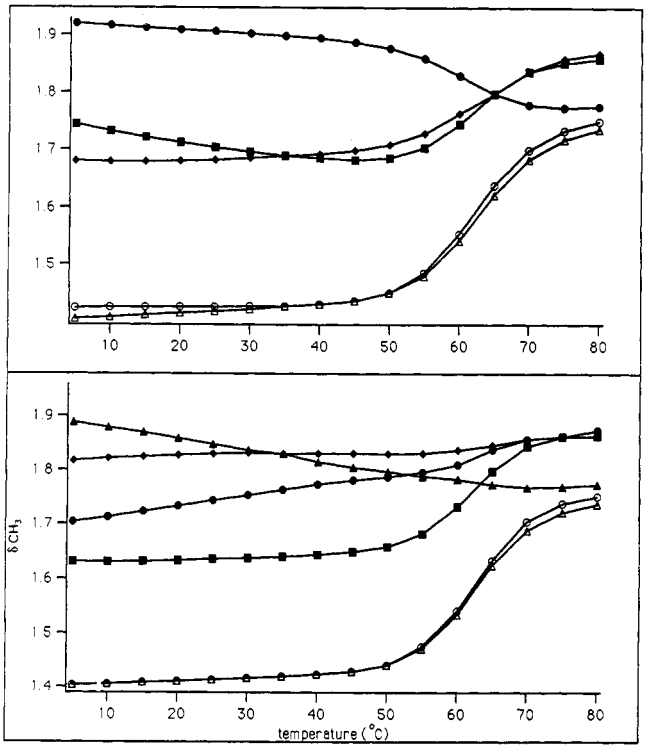

FIGURE 4: Temperature dependence of thymidine CH_3 chemical shifts in T3L (top) and T4L (bottom). A stem melting temperature of 62 °C is estimated for both hairpins. Symbols: (○) T4; (△) T10; (●) T_a; (♦) T_b; (■) T_c; (▲) T_d.

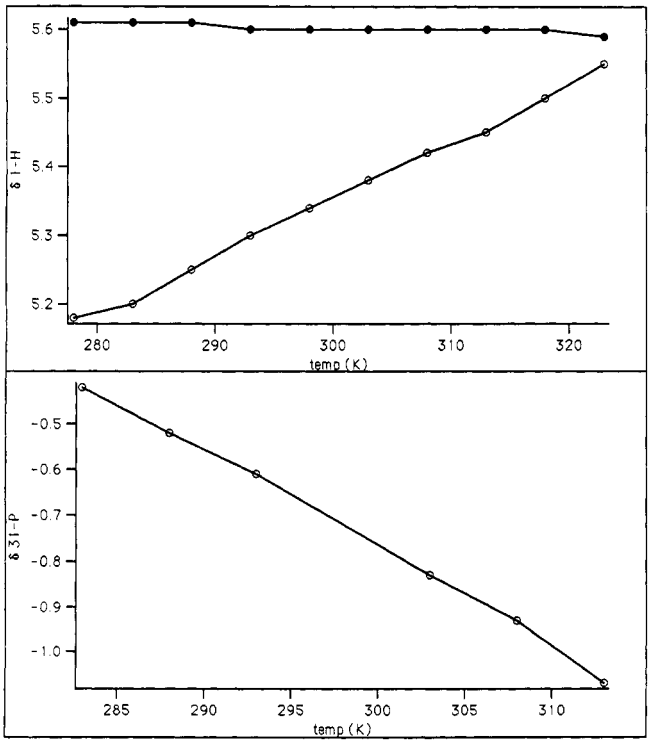

FIGURE 5: Both the H1′ resonance of C7 (a, top) and the ^{31}P resonance for C7pG8 (b, bottom) show abnormal sensitivity to temperature. For C7(H1′) (○), the dependence of G2(H1′) (●) is shown for comparison.

spectrum. Dihedral HCOP angles of 180° (β^+) and −60° (β^t) are expected to result in J_{HP} = 23 and 2 Hz, respectively (Lankhorst et al., 1984; Sklenar & Bax, 1987; van de Ven & Hilbers, 1988). The observed 15-Hz couplings are thus consistent with roughly 60% β^+, in agreement with the proportion estimated for the γ^t. Despite the large J_{HP} defining this interaction, the cross-peak is quite weak.

Table II: Approximate H3′–P Coupling Constants and ^{31}P Chemical Shifts[a]

	T3L		T4L	
phosphate	J (Hz)	δ	J(Hz)	δ
C1pG2	5.5	−1.10	5.5	−1.10
G2pA3	3.0	−1.08	nr	−1.07
A3pT4	nr	−1.45	~2	−1.46
T4pC5	nr	−1.20	nr	−1.25
C5pG6	4.0	−1.20	4.0	−1.11
G6pT_a	4.0	−1.02	~2	−1.27
T_apT_b	5.5	−1.65	~4	−0.97
T_bpT_c	4.5	−1.28	6.0	−1.55
T_cpT_d			6.0	−1.21
T_xpC7	5.5	−1.32	3.5	−1.57
C7pG8	4.0	−0.91	5.0	−0.51
G8pA9	2.0	−1.16	~2	−1.20
A9pT10	nr	−1.43	~2	−1.43
T10pC11	nr	−1.26	nr	−1.25
C11pG12	4.0	−0.94	4.0	−0.95

[a] Coupling constants >4 Hz were measured from the in-phase passive couplings observed along F_2 in H3′–H4′ DQF-COSY cross-peaks; those ≤4 Hz were estimated from the difference in H3′–H4′ cross-peak widths between DQF-COSY and DQF-COSY{^{31}P} spectra. Spectra were acquired with 0.7-Hz digital resolution in t_2, and J values are estimated to the closest 0.5 Hz. nr = coupling not resolved.

In T4L, a similar set of unusual cross-peaks is observed, although the step having a high proportion of γ^t and β^+ occurs at T_d rather than at C7. As the H4′–H5′ and H4′–H5″ cross-peaks for T_a are quite close to the diagonal in T4L, the disposition of the torsions at this step is not well determined from the DQF-COSY data, although regular values are indicated from the one resolved resonance. The γ and β torsions for other residues in both hairpins appear to fall within normal B-form ranges, based on the resolved H4′ and H5′/H5″ resonances.

The proportions of B_I (ϵ^t,ζ^-) and B_{II} (ϵ^-,ζ^t) phosphate conformers within regular double-helical segments can be estimated from the values of $J_{H3'-P}$ (Powers et al., 1989), with small couplings (2–3 Hz) reflecting B_I and large couplings (ca. 10 Hz) reflecting B_{II} phosphates due to the corresponding ϵ values. The H3′–P coupling constants were estimated from the in-phase passive splittings of the H3′–H4′ cross-peaks in the DQF-COSY spectra or from the difference between the H3′–H4′ cross-peak widths in the DQF-COSY and DQF-COSY{^{31}P} spectra when the couplings were not resolved. The majority of the resonances show H3′–P couplings of 4 Hz or less, typical of B_I phosphates. In both hairpins, C1 shows J = 5.5 Hz, suggesting conformational flexibility at the terminal pyrimidine. Larger values of $J_{H3'-P}$ are common within the loop segments (Table II), although the δ_P values suggest that this is due to phosphate conformations other than canonical B_I and B_{II}. The B_{II} conformer is expected to have δ_P substantially downfield from that of the B_I conformer due to the presence of ζ^t (Gorenstein & Luxon, 1979), whereas the hairpin loop phosphates showing enlarged $J_{H3'-P}$ resonate substantially upfield of the stem phosphates.

Model Building. An initial model for T3L was built using standard B-form parameters, without purposeful placement of the loop thymidine residues. Constrained molecular dynamics using 137 interproton distance constraints (46 sequential, 91 intranucleotide) derived from an independent spin pair analysis (ISPA) of the NOESY data and torsional constraints to fit the sugar pucker and phosphate data was used to move the model into rough agreement with the NMR data. The ISPA data set included 14 sequential distances to loop thymidines. This structure was then refined using the

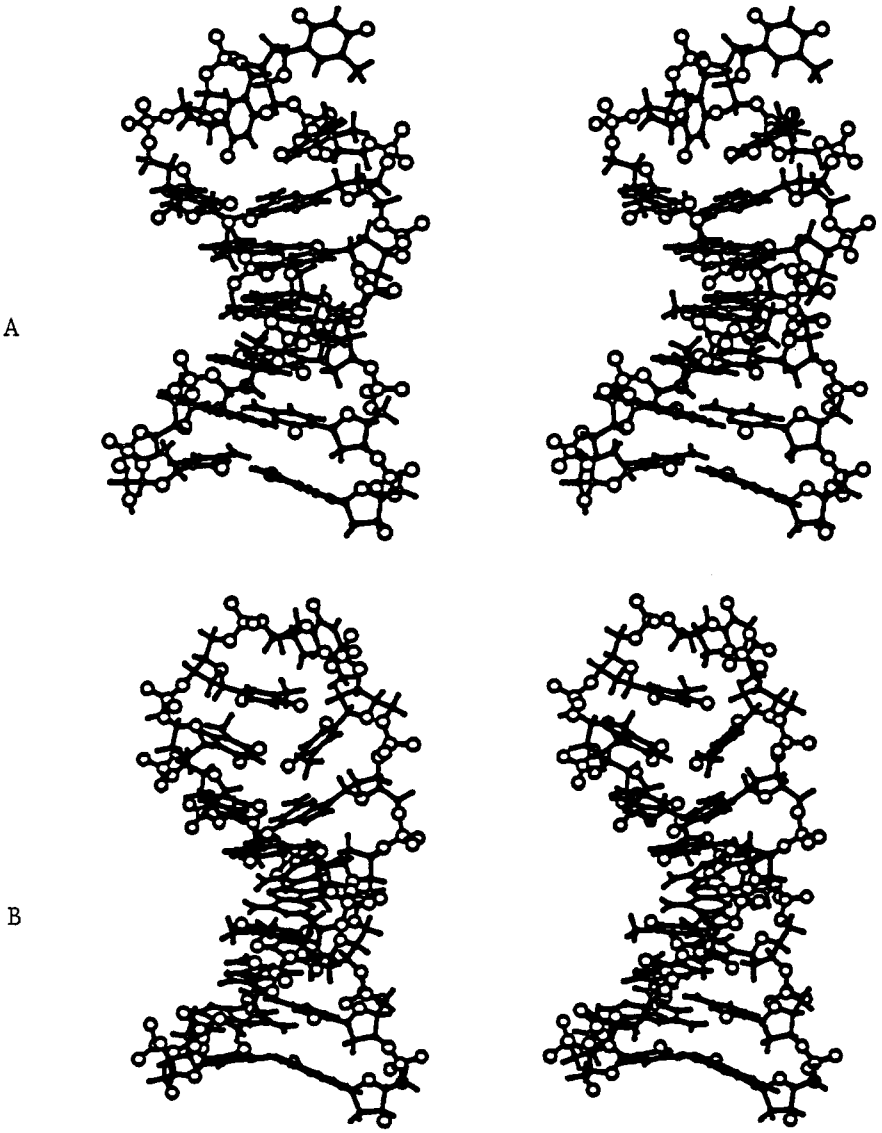

FIGURE 6: Stereo drawings of models for hairpins derived from MORASS refinement of NOESY data combined with backbone torsion constraints: (A) T3L; (B) T4L-1.

hybrid volume matrix relaxation analysis program MORASS. The agreement between the back-calculated NOESY spectrum and the experimental NOESY spectrum at t_{mix} = 100 ms is typical for that observed previously for simple DNA duplexes (Meadows et al., 1991), where percent errors in volume of 25–42% were observed. The fit appears reasonable, particularly considering the reliability of the present cross-peak volume integrations, which differed by as much as 100% when measured on opposite sides of the diagonal. It seems unreasonable in this case to expect a more precise fit than this for individual volumes.

The resulting T3L model (Figure 6A) has T_a and T_b roughly continuing the helical stack off of G6 and a sharp break at T_c. The glycosidic angle for G6 is high anti (χ = –84°), resulting in a twist of the sugar at this position. This conformation is dictated by several pieces of data, most notably a weak sequential NOE between C5 H6 and G6 H1′ and an unusually strong internal NOE between H8 and H2″, which yields an estimated interproton distance of 2.78 Å.

Two different loop-folding patterns were used as starting structures for refinement of T4L. The first (T4L-1) derived from distance geometry results obtained in this laboratory. T4L-1 (Figure 7a) has T_b folded toward the minor groove and T_c nearby T_a. This folding is enforced by the observation of nonsequential NOEs between T_a(H1′)·T_c(CH$_3$), T_a(H3′)·T_c(CH$_3$), and T_a(H6)·T_c(CH$_3$). The second model (T4L-2, Figure 7b) was derived from the previously proposed folding pattern for d[CGCG-TTTT-CGCG] (Hare & Reid, 1986) with the inclusion of reasonable backbone torsion angles. Both loop models were refined using 129 NOESY distance constraints (45 sequential, 84 intranucleotide) and torsional constraints as described above. The data set included 14 sequential distances to loop residues. Somewhat surprisingly, the two models were equally consistent with the NOESY data. T4L-1 gave RMS_{vol}(exp) = 45% and RMS_{vol}(the) = 38%, while T4L-2 gave RMS_{vol}(exp) = 37% and RMS_{vol}(the) = 46%. *R*-Factors of 20% were calculated for both models. It is thus not possible to distinguish the T4L-1 and T4L-2 folding motifs on the basis of NOESY data alone.

Examination of backbone torsions led to adoption of T4L-1 as the preferred folding motif for T4L. While it was possible to reconcile the NOESY distance data, the ^{31}P chemical shift data, and the backbone torsion data described above in the T4L-1 model, the T4L-2 model requires γ^t at T_c rather than T_d (Hare & Reid, 1986). Attempts to enforce the experimental torsion angles in the T4L-2 model led us to structures with high constraint energies.

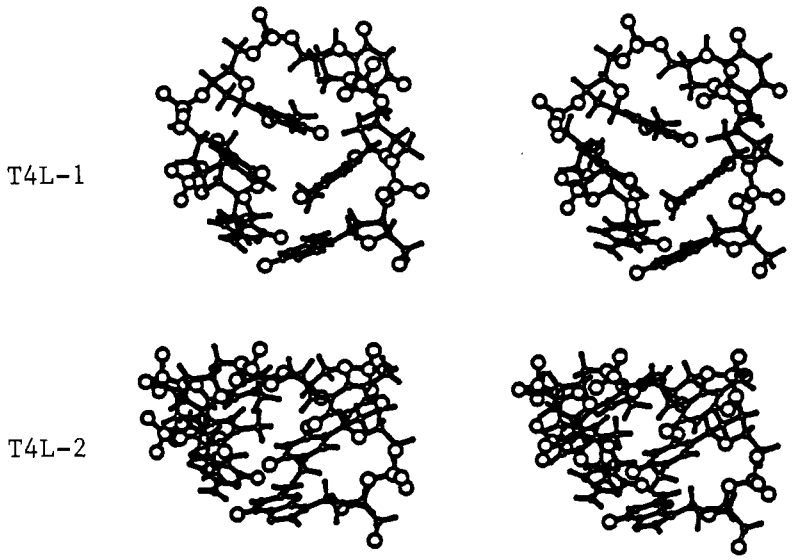

FIGURE 7: Stereo drawings of the two loop conformers found to fit the NOESY data for T4L. Both T4L-1 (a, top) and T4L-2 (b, bottom) give equivalent fits to the NOESY data by MORASS analysis, yet T4L-2 does not easily allow the required backbone torsional constraints.

The final T4L-1 model from hybrid matrix relaxation refinement (Figure 6B) shows stem conformational properties to be quite similar to that in T3L. As in T3L, G6 adopts a high anti conformation, with $\chi = -95°$. The reason for this behavior in both hairpins is unclear at present but may be related to dynamic behavior of the adjacent loop segments.

Molecular Mechanics Analysis of Phosphate Conformers. To probe the energetic feasibilities of C7pG8 phosphate conformers which might be involved in the observed flexibility at this step, and to probe the origins of the difference in flexibility between T3L and T4L, the three possible (ζ,α) conformers at C7pG8 were built by constraining these torsions to either –60° or 180° during minimization (constrained by refined NOESY distances and torsions) of the final T3L and T4L models, followed by unconstrained minimization to relax the structures. T3L gave high constraint energies for the (ζ^t,α^-) and (ζ^-,α^t) models, and both subsequently relaxed toward (ζ^-,α^-) structures with (ζ^t,α^-) moving to (–133°, –92°) and (ζ^-,α^t) moving to (–91°, –106°). In comparison, the (ζ^-,α^-) structure was stable and relaxed to (–83°, –93°). T4L, on the other hand, gave two distinct conformers at C7pG8 upon relaxation. The (ζ^-,α^-) and (ζ^t,α^-) models moved toward (ζ^-,α^-) structures of equivalent energy (121 kcal/mol) upon relaxation, (ζ^-,α^-) moving to (–102°, –71°) and (ζ^t,α^-) moving to (–119°, –69°). The (ζ^-,α^t) model relaxed to a structure of somewhat higher energy (126 kcal/mol) having (–28°, 179°).

Similar studies were undertaken to determine the probable values of ϵ at T_cpT_d in T4L in the (β^t,γ^+) and (β^+,γ^t) conformers. In both conformers the phosphate was constrained as (ζ^-,α^-) to account for the observed value of δ_P and to accommodate the local steric environment. Constrained minimization followed by relaxation gave $\epsilon = 25°$ for (β^t,γ^+) and $\epsilon = 135°$ for (β^+,γ^t). An equal mixture of these two conformers would reproduce the observed $J_{H3'-P}$ of 6 Hz reasonably well.

DISCUSSION

The data presented here provide a direct comparison of TTT and TTTT DNA hairpins having identical stem sequences and so allow a direct determination of the effect of hairpin loop size on the conformational properties of the adjacent double-helical DNA. The data also provide some information on hairpin dynamics based on approximate coupling data and back-calculation of NOESY cross-peak intensities. Finally, a more detailed picture of the TTTT hairpin loop emerges from consideration of both NOESY distance data and backbone torsion angle constraints.

The backbone flexibility observed at defined points in the hairpin loops suggests that it may not be possible to define a single hairpin structure to each molecule. Each of the hairpins studied here shows evidence of one highly flexible γ torsion, at C7 in T3L and at T_d in T4L, which adopts roughly equal proportions of the standard γ^+ and less common γ^t conformers. These linkages are also characterized by a very large coupling between the H5″ proton and phosphorus, which suggests a similar distribution of β^t and β^+ conformers. These results suggest that a correlated transition from the standard (β^t,γ^+) to (β^+,γ^t) is occurring readily at these steps (Figure 8). There is molecular dynamics evidence in double-helical segments to support a correlated transition between (α^-,β^t,γ^+) and (α^t,β^+,γ^t) (Beveridge et al., 1990), yet this type of transition seems unlikely in the present case given the prediction that the phosphorus in the α^t conformer would show a substantial downfield chemical shift (Gorenstein & Luxon, 1979). The observed δ_P values at these phosphates are typical of gauche conformers at α and ζ, however. Model building indicates that both (β,γ) conformers can be accommodated with the standard (ζ^-,α^-) torsions and that the transition can occur with very little motion of the nucleosides themselves due to the compensatory changes in adjacent torsion angles. Interpretation of NOE interactions to these nucleotides may nevertheless be compromised by this observed backbone mobility. It is unlikely that this flexibility would be apparent in analyses based solely upon NOESY data. The flexibility of these linkages appears to be the result of a lack of stacking interaction with the 5′-neighboring nucleotide, as T_c lacks a 5′-stacking partner in T3L while T_d lacks such a partner in T4L. This may relax some of the conformational constraints on the internucleotide linkages.

While H3′–P couplings of 2–4 Hz are observed for stem phosphates, consistent with normal B-form values for the correlated torsions ϵ and ζ (Powers et al., 1990), several loop phosphates show somewhat enlarged couplings of 5.5–6 Hz. The upfield δ_P values suggest that these larger couplings are not due to an increased proportion of the B_{II} phosphate

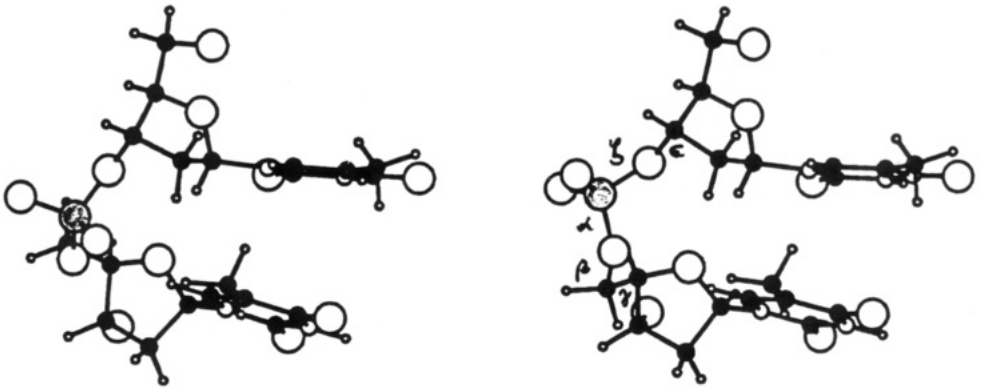

FIGURE 8: Interconversion of (β^t,γ^+) (left) and (β^+,γ^t) (right) conformers postulated to be occurring at the T9–C10 step in T3L and the T9–T10 step in T4L. The phosphate can flip without substantial changes in the nucleoside positions.

conformer (Gorenstein & Luxon, 1979). Modeling suggests instead that ϵ adopts atypical values at these loop positions without corresponding changes in ζ. In T4L, steric considerations together with δ_P require (ζ^-,α^-) at T_cpT_d for both conformers. When minimized with these torsional constraints and the NOESY-derived distances, the (β^t,γ^+) conformer has $\epsilon = 25°$, while the (β^+,γ^t) conformer has $\epsilon = 135°$. An equal mix of these conformers predicts $J_{H3'-P}$ near 8 Hz. This is larger than the observed 6 Hz but probably represents a good agreement given the likely accuracy of the model angles. Both (β,γ) conformers show $\epsilon = 119°$ at T_b–T_c, in agreement with the observed $J_{H3'-P}$ of 6 Hz at that position and (ζ^+,α^-) in agreement with the δ_P. These results suggest that ϵ and ζ are not as strongly correlated within the loop segment as they are in double-helical segments, perhaps due to the lack of base stacking as a conformational constraint and the need to span a different distance between nucleotide units.

Keeping the caveats of flexibility discussed above and previous demonstrations that multiple conformers of hairpin loops may be mutually consistent with the same set of NOESY data (Erie et al., 1993) in mind, the data can be used to provide an approximate view of the hairpin structures. Previous ^{13}C relaxation measurements have indicated lower order parameters for thymidines in TTGTT hairpin loops than for those in double-helical stems (Williamson & Boxer, 1989a), and molecular dynamics simulations have suggested different order parameters for different interproton vectors within a double helix (Koning et al., 1991). A single isotropic correlation time was used for the current refinement process, as comparison of H6–CH_3 distances calculated for loop and stem thymidines indicated agreement (±0.2 Å) well within the anticipated limits of the NOE. The effects of the lower order parameters on the distance estimates are calculated to be approximately 10% for a DNA molecule of this size and are thus only slightly outside the usually accepted error limits on NOESY distances. Hybrid relaxation matrix analysis of the NOESY data using a single correlation time indicates a reasonable fit of the final models to the experimental data based on likely integration errors. Nonetheless, the observed mobility of the loops creates difficulties in model building and analysis of the accuracy of the NOESY-derived structure, and a single definitive model for the hairpin loop structures may not be possible.

For T3L, the NOESY-derived loop structure consists of continued approximate stacking of T_a and T_b off the 3′ end of the stem, with T_c acting to close the gap to the other side of the stem, consistent with the predictions of Haasnoot et al. (1986). The CH_3 and H6 resonances of T_a occur at values typical of unstacked thymidine (thymidine itself shows δ 1.90 and 7.67 for these protons). It appears from the model that T_a does not stack in the normal B-form manner but adopts an average position where the base protons are not effectively shielded by G6. Upon melting of the hairpin loop structure, the base protons of T_a adopt chemical shifts more typical of interaction with a neighboring shielding purine residue. In the folded form, the base protons of T_b and T_c are shielded relative to free thymidine, although to a lesser extent than they would be in a B-form stack. This is apparently a result of the unusual orientation of these residues in the loop, as melting of the hairpin results in deshielding. It might be argued from the melting data that T_b and T_c appear to be stacked, while T_a is not, but this is not consistent with either the NOESY or the backbone conformation data. The proposed T3L model fits the observed flexibility of the phosphate backbone, as T_c is essentially free of helical constraints, whereas T_a and T_b should show less freedom due to weak stacking interactions. A DNA TTT hairpin of nearly identical stem sequence has been recently reported to adopt a quite different structure (Boulard et al., 1991). This model predicts γ^t for all three loop T residues as well as C7 and is clearly inconsistent with the *J*-coupling data presented here. The inconsistencies may be the result of the higher temperature and cation concentration conditions used for the NMR measurements.

The T4L-1 loop structure is similar to the structure proposed earlier for a TTTA hairpin (Blommers et al., 1991), in that T_b folds back toward the minor groove. The T4L-2 loop structure resembles earlier TTTT models (Hare & Reid, 1986; Hassnoot et al., 1986; Blommers et al., 1991), in that T_b folds toward the major groove. Both conformations of T4L differ from those observed by X-ray crystallographic analyses of a simple DNA hairpin (Chattopadhyaya et al., 1988) and of a dG tetraplex connected by TTTT loops (Kang et al., 1992). The latter structure is in agreement with the predictions of Haasnoot et al. (1986), but both models are inconsistent with the data reported here. The T4L-1 model rationalizes several otherwise puzzling observations: (1) T_b resonances are relatively insensitive to temperature, even at the T_m, and are in general only slightly shielded relative to free thymidine. Stacking interactions give rise to shielding effects, whereas minor groove binding gives rise to deshielding effects (Blommers et al., 1991). The chemical shift data thus are consistent with T_b being neither stacked as in T4L-2 nor held tightly in the minor groove as in the TTTA hairpin but rather exposed to solvent. (2) T_b is the most reactive loop thymidine toward oxidation by $KMnO_4$. At relatively low extents of total DNA damage (77% of the DNA undamaged), cleavage at T_b makes up 31% whereas cleavage at T_a makes up only 17% of the total damage. T_c and T_d are damaged equally (20–22%). As the total DNA damage increases, T_a and T_b make up larger

percentages of the total due to multiple reactions (S. M. Baxter, unpublished results). These results suggest a special reactivity of T_b toward $KMnO_4$ which is not explainable by either a stacked or groove-bound model.

The temperature dependence of loop thymidine base resonances in T4L is more complex than that in T3L, but it in general appears to fit the proposed T4L-1 model. The stacked residues T_a and T_c are deshielded upon melting. Residue T_d is essentially unstacked in the hairpin form and becomes shielded upon melting. Both T_a and T_d show substantial temperature dependences well below the melting point of the structure, suggesting substantial conformational mobility in T4L which is not apparent in T3L.

The pattern of δ_P values observed for loop phosphates mirrors that observed in the TTTA hairpin, with the exception of T_dpC7. This phosphate resonates within the normal envelope of stem resonances in the TTTA hairpin but gives rise to a substantially upfield-shifted signal in T4L. This appears to reflect different conformational flexibility between the two hairpins at this position. The T_c–T_d step is the most flexible in the TTTT loop on the basis of the observed J couplings. On the basis of NOESY distance estimates, unusual DQF-COSY cross-peak fine structure, and a detailed conformational search, pure γ^t was determined for A_d in the TTTA hairpin (Blommers et al., 1991), although no evidence was observed for a corresponding gauche conformer at β. Analyzed as a single-state model, T_cpA_d was assigned as $(\epsilon^-,\zeta^+,\alpha^+,\beta^t,\gamma^t)$. In contrast, the data presented here for TTTT are more consistent with a two-state model for T_cpT_d where $(\epsilon^+,\zeta^-,\alpha^-,\beta^t,\gamma^+)$ and $(\epsilon^+,\zeta^-,\alpha^-,\beta^+,\gamma^t)$ interconvert. The dynamic differences in these two four-member hairpins at this position may result from decreased loop flexibility due to the Hoogsteen A·T pair closing the TTTA loop, together with the shift of the primary stacking partner for T_c from T_a in T4L to A_d in the TTTA hairpin. The balance between the thermodynamically favored stacking of loop bases from the 3′ end of the helical stem and the geometrically favored stacking on the 5′ end of the stem has been noted (Haasnoot et al., 1987).

Significant distortions of the helix are noted at the G6·C7 base pair in both T3L and T4L, although this conclusion must be tempered by the realization that the flexibility of the adjacent loop segments may influence the reliability of the NOESY analysis in this region of the molecule. G6 adopts a high antiglycosidic conformation in both models. This exposes G6(H2″) more directly to the anisotropy of T_a in both hairpins, such that the positioning of T_a greatly influences the chemical shift of G6(H2″), with a lesser effect on G6-(H2′). G6(H2″) resonates upfield of G6(H2′) in T3L, which is unusual. This behavior is readily rationalized by the model, which predicts that the ring of T_a will effectively shield G6-(H2″). The T4L models, in contrast, show G6(H2″) to lie under the methyl of T_a where it should be less shielded by the T_a ring, as is in fact observed. Both NOESY distance estimates and proton chemical shift data thus support the predicted distortion at G6.

The ^{31}P chemical shift appears to be a sensitive indicator of conformational differences between the two stem segments. Significant differences between phosphate chemical shifts are noted beginning at the T4·A9/C5·G8 step ($\Delta\delta_P = 0.05$ ppm). Proton chemical shifts begin to differ only within the C5·G8 base pair, and the magnitudes of these differences are generally small. This suggests that the effect of the loop segments may extend as far as the phosphates between the two base pairs adjoining the loops.

The behavior of the phosphate connecting C7 to G8 demonstrates that the effect of a hairpin loop on the conformational dynamics of the adjacent stem segment is a complex function of loop size and adjacent stem sequence. An essentially identical chemical shift to that observed in T4L has been reported for the equivalently positioned phosphate in the five-member hairpin d[CGCG-TTGTT-C**p**GCG] (Williamson & Boxer, 1989a) and has been suggested to be caused by a fast exchange of this phosphate between (ζ^t,α^-) and (ζ^-,α^-) conformations. Our data on T4L indicate that this phosphate is indeed undergoing facile interconversion, although (α^t,ζ^-) is predicted as the favored downfield conformer by molecular mechanics. The symmetry of the torsion angle/chemical shift correlation makes the pair of (α^-,ζ^t) and (α^t,ζ^-) conformers indistinguishable on the basis of the observed δ_P. The observed chemical shift is consistent with a roughly equal mixture of conformers at C7pG8 in T4L at 25 °C (Gorenstein & Luxon, 1979). C7pG8 is also the lowest field phosphate in T3L, although with a difference of only 0.19 ppm from C1pG2, the effect is essentially absent. Molecular mechanics evaluation of the phosphate conformers suggests that there is very little freedom at this position in T3L, at least as long as the loop-folding pattern remains constant. The stem in T3L thus appears to be less flexible at the junction than in T4L, perhaps due to tighter conformational constraints imposed by the smaller connecting loop in T3L.

The conformational freedom observed in T4L at this position is dependent on the stem sequence. An unusual δ_P was not observed for the hairpin d[CTGCTC-TTGTT-G**p**AGCAG] (Williamson & Boxer, 1989b), and we have observed that the equivalent ^{31}P resonance in d[GCAAGC-TTTT-G**p**CTTGC] occurs at a typical B_I value of −1.07 ppm (S. M. Baxter, unpublished data). Such data imply that terminating the TTTT loop segment on the 3′ end with a purine gives rise to a less flexible stem. This may be manifested as a greater difficulty in initiating stem melting at the hairpin loop. It has been noted, in agreement with this idea, that changing the closing base pair from G·C to C·G leads to an increase in hairpin melting temperatures in several DNA tetraloops (Antao & Tinoco, 1992).

The H1′ resonance of C7 also shows a high temperature sensitivity. This effect was also noted for the larger -TTGTT- hairpin sequence (Williamson & Boxer, 1989a). We have noted in related work that this effect is also sequence dependent, such that TTTT loops adjacent to C·G rather than G·C pairs do not show temperature-sensitive H1′ resonances (Ashley & Kushlan, 1991). While these results point toward a connection between this effect and the sensitivity at phosphorus just discussed, this does not seem to be the case since the effect on C7 H1′ is noted in both T3L and T4L, whereas the effect on phosphorus is unique to T4L. Given the positioning of C7 H1′ in the models of T3L and T4L, it is more likely that the temperature sensitivity reflects for the most part the dynamics of the adjacent loop bases, T_c in T3L or T_d in T4L. If so, this suggests that the corresponding loop dynamics in loops adjacent to C·G rather than G·C pairs may be significantly different, reflecting perhaps the difference in stacking energies between G and C. The folding patterns of T_n loops may thus be different for stems ending in C·G and in G·C pairs.

In summary, NMR experiments on two DNA hairpins of identical stem sequence have provided information on the conformational and dynamic properties of TTT and TTTT hairpin loops and the effects of these loops on the structure and dynamics of the adjacent double-helical DNA stem. Within the loop segments, both hairpins show single nucleotides

having substantial backbone flexibility at the 3′ end of the loop. The most substantial effects on the stem are localized to the base pair at the stem–loop junction, although chemical shift comparison indicates smaller effects at the penultimate base pair as well. The smaller TTT loop appears to reduce the conformational freedom in the adjacent stem, whereas the TTTT loop shows behavior quite similar to previously described five-membered loops. It may be that many of the observed effects of hairpin loop size on the binding and action of proteins at the adjacent stem segment result primarily from such changes in stem dynamics rather than gross structural alterations.

ACKNOWLEDGMENT

The 600-MHz NMR Facility was funded by grants from the W. M. Keck Foundation, NIH, NSF, and Northwestern University. We thank Dr. D. Gorenstein for the generous gift of MORASS.

SUPPLEMENTARY MATERIAL AVAILABLE

Two tables listing the NOESY cross-peaks used in the refinement of the T3L and T4L structures, along with the experimental and theoretical volumes (8 pages). Ordering information is given on any current masthead page.

REFERENCES

Amaratunga, M., Snowden-Ifft, E., Wemmer, D. E., & Benight, A. S. (1992) *Biopolymers 32*, 865–879.

Antao, V. P., & Tinoco, I., Jr. (1992) *Nucleic Acids Res. 20*, 819–824.

Ashley, G. W., & Kushlan, D. M. (1991) *Biochemistry 30*, 2927–2933.

Beveridge, D. L., Subramanian, P., Jayaram, B., Swaminathan, S., & Ravishankar, G. (1990) in *Structure & Methods, Volume 3: DNA & RNA* (Sarma, R. H., & Sarma, M. H., Eds.) pp 79–112, Adenine Press, Schenectady, NY.

Blommers, M. J. J., van de Ven, F. J. M., van der Marel, G. A., van Boom, J. H., & Hilbers, C. W. (1991) *Eur. J. Biochem. 201*, 33–51.

Boulard, Y., Gabarro-Arpa, J., Cognet, J. A. H., Le Bret, M., Guy, A., Teoule, R., Guschlbauer, W., & Fazakerley, G. V. (1991) *Nucleic Acids Res. 19*, 5159–5167.

Chattopadhyaya, R., Ikuta, S., Grzeskowiak, K., & Dickerson, R. E. (1988) *Nature 334*, 175–179.

Chazin, W. J., Wuthrich, K., Hyberts, S., Rance, M., Denny, W. A., & Leupin, W. (1986) *J. Mol. Biol. 190*, 439–453.

Erie, D. A., Jones, R. A., Olson, W. K., Sinha, N. K., & Breslauer, H. J. (1989) *Biochemistry 28*, 268–273.

Erie, D. A., Suri, A. K., Breslauer, K. J., Jones, R. A., & Olson, W. K. (1993) *Biochemistry 32*, 436–454.

Germann, M. W., Kalisch, B. W., Lundberg, P., Vogel, H. J., & van de Sande, J. H. (1990) *Nucleic Acids Res. 18*, 1489–1497.

Giessner-Prettre, C., & Pullman, B. (1977) *J. Theor. Biol. 65*, 189–201.

Gorenstein, D. G., & Luxon, B. A. (1979) *Biochemistry 18*, 3796–3804.

Gorenstein, D. G., Meadows, R. P., Metz, J. T., Nikonowicz, E. P., & Post, C. P. (1990) in *Advances in Biophysical Chemistry* (Bush, C. A., Ed.) pp 47–124, JAI Press, Greenwich.

Haasnoot, C. A. G., Hilbers, C. W., van der Marel, G. A., van Boom, J. H., Singh, U. C., Pattabiraman, N., & Kollman, P. A. (1986) *J. Biomol. Struct. Dyn. 3*, 843–857.

Hare, D. R., & Reid, B. R. (1986) *Biochemistry 25*, 5341–5350.

Hare, D. R., Wemmer, D. E., Chou, S. H., Drobny, G., & Reid, B. R. (1983) *J. Mol. Biol. 171*, 319–336.

Ikuta, S., Chattopadhyaya, R., Ito, H., Dickerson, R. E., & Kearns, D. R. (1986) *Biochemistry 25*, 4840–4849.

Kang, C., Zhang, X., Ratliff, R., Moyzis, R., & Rich, A. (1992) *Nature 356*, 126–131.

Kim, S.-G., Lin, L.-J., & Reid, B. R. (1992) *Biochemistry 31*, 3564–3574.

Kollman, P. A., Weiner, P. K., & Dearing, A. (1981) *Biopolymers 20*, 2583.

Koning, T. M. G., Boelens, R., van der Marel, G. A., van Boom, J. H., & Kaptein, R. (1991) *Biochemistry 30*, 3787–3797.

Lankhorst, P. P., Haasnoot, C. A. G., Erkelens, C., & Altona, C. (1984) *J. Biomol. Struct. Dyn. 1*, 1387–1405.

Mayo, S. L., Olafson, B. D., & Goddard, W. A., III (1990) *J. Phys. Chem. 94*, 8897–8909.

Meadows, R. P., Kaluarachchi, K., Post, C. B., & Gorenstein, D. G. (1991) *Bull. Magn. Reson. 13*, 22–48.

Nikonowicz, E. P., Meadows, R. P., & Gorenstein, D. G. (1990) *Biochemistry 29*, 4193–4204.

Paner, T. M., Amaratunga, M., & Benight, A. S. (1992) *Biopolymers 32*, 881–892.

Powers, R., Olsen, R. K., & Gorenstein, D. G. (1989) *J. Biomol. Struct. Dyn. 7*, 515–556.

Senior, M. M., Jones, R. A., & Breslauer, K. J. (1988) *Proc. Natl. Acad. Sci. U.S.A. 85*, 6242–6246.

Sklenar, V., Miyashiro, H., Zon, G., Miles, H. T., & Bax, A. (1986) *FEBS Lett. 208*, 94–98.

States, D. J., Haberkorn, R. A., & Ruben, D. J. (1982) *J. Magn. Reson. 48*, 286–292.

Tebby, J. C. (1987) in *Phosphorus-31 NMR Spectroscopy in Stereochemical Analysis* (Verkade, J. G., & Quin, L. D., Eds.) pp 1–60, VCH Publishers, Deerfield Beach, FL.

Williamson, D., & Bax, A. (1988) *J. Magn. Reson. 76*, 174–177.

Williamson, J. R., & Boxer, S. G. (1989a) *Biochemistry 28*, 2819–2831.

Williamson, J. R., & Boxer, S. G. (1989b) *Biochemistry 28*, 2831–2836.

Williamson, J. R., & Celander, D. W. (1990) *Nucleic Acids Res. 18*, 379.